

Received April 10, 2020, accepted April 19, 2020, date of publication April 22, 2020, date of current version May 7, 2020.

Digital Object Identifier 10.1109/ACCESS.2020.2989479

Multiple Transient Transitions Behavior Analysis of a Double Memristor's Hidden System and Its Circuit

CHUANHONG DU¹, LICAI LIU¹ , (Member, IEEE), SHUAISHUAI SHI², AND YONG WEI³

¹School of Electronic and Information Engineering, Anshun University, Anshun 561000, China

²School of Information Engineering, Guizhou University of Engineering Science, Bijie 551700, China

³School of Electronics and Information, Yangtze University, Jinzhou 434023, China

Corresponding author: Licai Liu (liulicai1981@126.com)

This work was supported in part by the Growth Project of Young Scientific and Technological Talents in Guizhou for Colleges and Universities under Grant [KY [2019] 160], in part by the Natural Science Research Youth Project of the Department of Education of Guizhou Province of China under Grant [KY [2015] 470], and in part by the Tripartite Joint Funds for Science and Technology Department of Guizhou Province of China under Grant [LH [2015] 7697].


ABSTRACT In this paper, a low-dimensional hidden nonlinear system is constructed by replacing two linear resistors of a simple integrating circuit with two active memristors. The system was analyzed in detail by using the Lyapunov exponent, 0-1 Test, Poincaré map, phase diagram, power spectral density diagram, time-domain waveform, and chaotic characteristic diagram. The results show that the system can oscillate by itself under zero initial conditions, and there are various transient transition behaviors, such as from chaos to limit cycle, chaos to quasi-periodic, quasi-periodic to another quasi-periodic transition, quasi-periodic to periodic transition. Besides, these transient processes themselves include 2, 3, 4, and 5 different states respectively, showing multiple transient transitions behavior, which are not reported in the related literature. It is also found that the initial states of these transition states have rich symmetrical attractors and the stable state is multistability. In addition, the global entropy analysis method is adopted to test the universal existence of transient behaviors, which demonstrates that the system has rich nonlinear characteristics. Finally, the memristive circuit verifies the system's physical feasibility and enriches the application of memristors in circuit theory.

INDEX TERMS Active memristor, hidden attractor, multiple transient transitions, chaos, simple integrating circuit.

I. INTRODUCTION

As a new type of element, the memristor has richer non-linear properties than other linear components. The circuit system composed of a memristor is different from ordinary circuits. It may become an important factor affecting system performance, which has attracted many scholars' interest. At present, memristor has been widely used in many fields, such as artificial neural networks, secure communication, new memory and so on, and some research results have been obtained [1]–[5]. In the past decade, some researchers have designed many kinds of memristive chaotic circuits by replacing Chua's circuit with memristors or standardizing Chua's diode in Chua's circuit [6]–[15]. In addition to Chua's

circuit, few studies have explored memristive chaotic systems based on various filter circuit systems [16]–[19]. Moreover, to increase the non-linear characteristics of the system, some researchers have introduced the memristor model into the original chaotic mathematical model by the means of adding nonlinear feedback terms [20]–[24], changing the circuit branch, adding feedback branches for the typical circuit system, replacing the linear resistance of the circuit, changing the topological structure of the circuit, so various new memristive chaotic systems are proposed [11], [18], [25]–[32]. Most of these memristive circuit systems belong to high-dimensional non-linear systems with a dimension of 4 or more, their circuit composition is complex and there are always many components. Only a few studies have reduced the dimension of the memristor chaotic system [19], [33]–[35]. In this paper, two memristors are used to replace the two linear resistors

The associate editor coordinating the review of this manuscript and approving it for publication was Di He .

in the simple integrating circuit. The circuit structure of the memristive system is relatively simple, and the number of components is less. Moreover, the mathematical model of the circuit system is simple and has only three dimensions. To date, there have been no attempts to study the integrating circuit composed of a single ideal operational amplifier. So, it is of great significance to obtain the memristive nonlinear system with non-equilibrium by replacing linear resistance in the integrating circuit.

Compared with the self-excited attractor system, the hidden chaotic system has some special nonlinear behaviors. For example, the hidden system has numerous equilibrium points or has a stable equilibrium point or even no equilibrium point, and the dynamic behavior of the hidden chaotic system is more dependent on the initial value. These interesting phenomena have been found and reported in many published studies [36]–[49]. Some hidden chaotic systems also have the characteristic of multistability, which is reported by many scholars [50]–[52]. Vaibhav Varshney and S. Sabarathinam *et al.* found the hidden behavior due to ‘periodic line invariant’ and analyzed the causes of multistable state in the reference [53]. Since the initial value is one of the key factors that affect the state of memristor, the sensitivity of the memristive chaotic system includes the sensitivity to the initial value of the memristor itself. Most of the systems composed of memristors have strong extreme multistability, that is, the phenomenon that an infinite number of attractors coexist [14], [28], [30], [54], [55]. Due to the introduction of negative input resistance, the system has no solution, the double memristive circuit system model based on the integrating circuit proposed in this paper is a typical hidden nonlinear system. More importantly, because the circuit system equation is mainly composed of two memristor equations, this nonlinear system appears to be more sensitive to the internal variables of the memristor. This makes the stable state of the system also behave as multiple attractors coexist at different initial values, the so-called multistability.

Transient transition behavior is a common nonlinear dynamic phenomenon, which has been reported in some existing literature. For example, Bao Han and Ning Wang *et al.* found a little-known transient process from cycle to chaos in the chaotic system that depends on initial conditions [25]. A. Ishaq Ahamed observed the chaotic oscillation phenomenon from transient hyperchaos to stable chaos in the model of MLC circuit [7]. Bocheng Bao and Han Bao have discovered three kinds of transient behaviors in a memristor hyperchaotic system. They are from transient hyperchaos to stable periods, from one transient hyperchaos attractor to another attractor with different dynamic amplitudes, from transient hyperchaos to stable chaos [54]. In the study of a multi-type quasi-periodic system with memristors, Licai Liu *et al.* observed the transient behavior from a weak chaotic state to a quasi-periodic limit cycle [55]. The transient nonlinear behaviors found in these reports are representative, and similar reports on transients are abundant [56]–[74]. However, these studies have only found that the chaotic

system has transient transition behavior under certain specific parameters. In other words, this type of transient behavior is a special state for the nonlinear system, rather than for other parameters or most parameters. In addition, there are only two kinds of transient state behavior reported in the existing reports, namely, only the initial state and the final state. In this paper, with the help of research methods such as a chaotic characteristic diagram, phase diagram, the Lyapunov exponent spectrum (LEs) and global entropy, it is proved that the transient process of the three-dimensional double memristive system has 2, 3, 4, and 5 different states respectively. And the transient behavior of the system is universal under different system parameters and initial values. The nonlinear system proposed in this paper has a wide range of transient behavior and reveals the existence of multiple transient transitions phenomena for the first time.

The structure of this paper is as follows. Section II gives a memristive circuit system model based on a simple integrating circuit and a new memristive hidden nonlinear system mathematical model. At the same time, using MATLAB to perform numerical simulation on the new system. Specifically, by analyzing the chaotic characteristic diagram, the initial state of the system is given as the system parameters and the initial value of the system change, and take 4×10^4 seconds simulation time as the system stable state. In Section III, it is proved that the transient transition behavior of the system is universal through some specific simulation examples. The existence of the transient transition behavior is confirmed by comparing the differences of the attractors in the two-dimensional phase plane projection diagram. In Section IV, four specific transient transition processes are introduced, which proves the existence of multiple transient transitions behavior. Since the system has different stable states under different initial value conditions, Section V declares that the system is multistable. In Section VI, the SE value of the system is analyzed from the perspective of global entropy. It further confirms that the transient transition behavior of the system is universal. In Section VII, the design process of the system's memristive unit circuit is given, and the memristive circuit is simulated and verified using Multisim software under specific system parameters. Section VIII summarizes the main research contents of this paper.

II. DOUBLE MEMRISTOR'S HIDDEN NONLINEAR SYSTEM

The common simple integrating circuit is shown in Fig. 1(a). In Fig. 1(a), the component *A* is an operational amplifier, *z* and *u* are the input signals of the linear resistance R_1 and R_3 respectively, *C* is the integrating capacitance, and u_o is the output signal of the integrator. According to Kirchhoff's current law, Equation (1) holds.

$$\left\{ \frac{du_o}{dt} = -\frac{1}{C} \left(\frac{1}{R_1}z + \frac{1}{R_2}u_o + \frac{1}{R_3}u \right) \right. \quad (1)$$

When the value of the linear resistance $R_1 = R_2 = R_3$, $\frac{du_o}{dt} = -\frac{1}{RC} (z + u_o + u)$. Here, *z* is used as the input signal, and it is also used as the independent variable of the

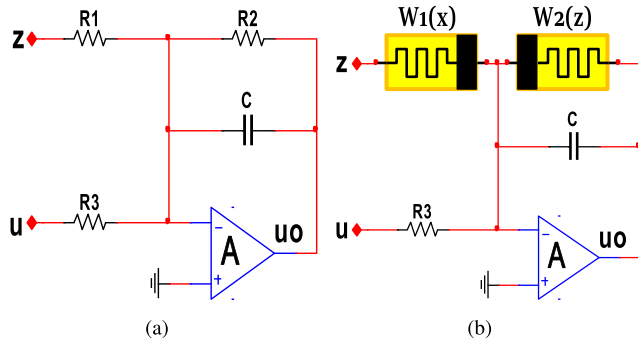


FIGURE 1. Circuit schematic: (a) simple integrating circuit; (b) double memristors circuit.

memductance values function $W_2(\cdot)$ for some flux-controlled memristor. It can be obtained $W_2(z)$. Using $W_2(z)$ and flux-controlled memristor $W_1(x)$ to replace R_1 and R_2 in Fig. 1(a), respectively, the double memristors circuit as shown in Fig. 1(b) is obtained. At this time, the output signal of the integrating circuit is

$$\left\{ \begin{aligned} \frac{du_o}{dt} &= -\frac{1}{C} \left(W_1(x)z + W_2(z)u_o + \frac{1}{R_3}u \right) \end{aligned} \right. \quad (2)$$

where $W_1(x)$ and $W_2(z)$ both use the memristive model in reference [75], so there are Equation (3) and Equation (4), in which the coefficients of equations m, n, p, q are all positive real numbers. Then Equation (5) can be obtained.

$$\left\{ \begin{aligned} i_1 &= W_1(x)z = (-m + n|x|)z \\ \frac{dx}{dt} &= z \end{aligned} \right. \quad (3)$$

$$\left\{ \begin{aligned} i_2 &= W_2(z)u_o = (-p + q|z|)u_o \\ \frac{dz}{dt} &= u_o \end{aligned} \right. \quad (4)$$

$$\left\{ \begin{aligned} \frac{dx}{dt} &= z \\ \frac{du_o}{dt} &= -\frac{1}{C} \left((-m + n|x|)z + (-p + q|z|)u_o + \frac{1}{R_3}u \right) \\ \frac{dz}{dt} &= u_o \end{aligned} \right. \quad (5)$$

Let $y = u_o, \xi = -\frac{u}{CR_3} \neq 0, e = \frac{\gamma}{C}, a = \frac{m}{\gamma}, b = \frac{n}{\gamma}, g = \frac{\lambda}{C}, c = \frac{p}{\lambda}, d = \frac{q}{\lambda}$, and $\gamma, \lambda > 0$, we can get the equation of the system as shown in Equation (6). Interestingly, the new system is a coupling of two flux-controlled $W_{\phi 1}(x), W_{\phi 2}(z)$ memristors proposed in reference [25]. In Equation (6), $a, b, c,$ and d are constant coefficients; x and z are the internal variables of the memristor; y is the state variable; the corresponding mathematical expressions of $W_{\phi 1}(x)$ and $W_{\phi 2}(z)$ are Equation (7) and Equation (8), respectively.

$$\left\{ \begin{aligned} \dot{x} &= z \\ \dot{y} &= e(a - b|x|)z + g(c - d|z|)y + \xi \\ \dot{z} &= y \end{aligned} \right. \quad (6)$$

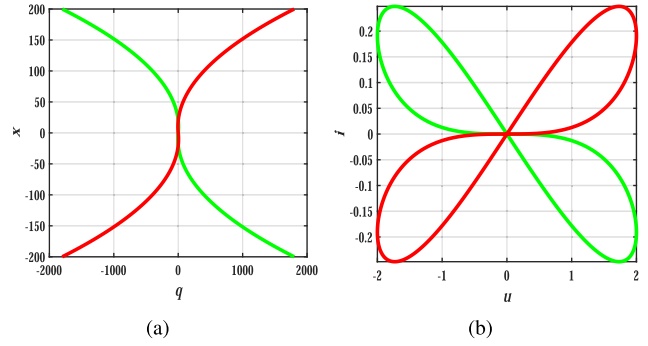


FIGURE 2. Two memristor model curve, $W_1(x)$ (red), $W_{\phi 1}(x)$ (green): (a) charge – flux; (b) voltage – current.

$$\left\{ \begin{aligned} i_1 &= W_{\phi 1}(x)z = (a - b|x|)z \\ \frac{dx}{dt} &= z \end{aligned} \right. \quad (7)$$

$$\left\{ \begin{aligned} i_2 &= W_{\phi 2}(z)y = (c - d|z|)y \\ \frac{dz}{dt} &= y \end{aligned} \right. \quad (8)$$

When $m = p = a = c = 1$, and $n = q = b = d = 0.1$, comparing the memristive model represented by Equation (3) and Equation (4) with the memristive model represented by Equation (7) and Equation (8), we can get Equation (9) and Equation (10). The characteristic curves of the memristive model represented by Equations (9) and (10) are plotted in Fig. 2. In Fig. 2, x is the flux and q is the charge, the red curve corresponds to Equation (9) and the green curve corresponds to Equation (10). The input signal in Fig. 2 uses a sine wave voltage with an amplitude of 2V, the frequency of the voltage is 0.3334Hz, the initial value $x_0 = 10$ V. It can be seen from Fig. 2 that the characteristic curve of the two memristor model is strictly symmetric, which is consistent with their mathematical models. Besides, when $m = p = a = c > 0$ and $n = q = b = d > 0$, there is an interval that the memductance values of both memristors are less than 0, as shown in Fig. 2(a), so W_i and $W_{\phi i}$ ($i = 1, 2$) belong to the active memristor. Comparing Equation (5) and (6), we will find an interesting phenomenon in the process of deriving the state equation of the system, that is, the active memristor introduced into the circuit evolves into another active memristor in the system state equation. This transformation method has never been reported in the relevant literature.

$$\left\{ \begin{aligned} W_1(x) &= -m + n|x| \\ q(x) &= \int_{-\infty}^x W_1(t) dt \end{aligned} \right. \quad (9)$$

$$\left\{ \begin{aligned} W_{\phi 1}(x) &= a - b|x| \\ q(x) &= \int_{-\infty}^x W_{\phi 1}(t) dt \end{aligned} \right. \quad (10)$$

The equilibrium points of system equation (6) can be obtained by solving Equation (11). Because $\xi \neq 0$, it can be seen that there is no solution for Equation (11), the system belongs to the hidden system without equilibrium point. The LEs could quantitatively determine the nonlinear behavior of

the system. Jacobian matrix (12) is needed to solve the LEs of the system by using the Wolf method [76].

$$\begin{cases} z = 0 \\ e(a - b|x|)z + g(c - d|z|)y + \xi = 0 \\ y = 0 \end{cases} \quad (11)$$

$$J = \begin{pmatrix} 0 & 0 & 1 \\ -bez \cdot \text{sign}(x) & g[c-d|z|] & e[a-b|x|] - dgy \cdot \text{sign}(z) \\ 0 & 1 & 0 \end{pmatrix} \quad (12)$$

For the system equation (6), select the system and simulation parameters: $e = 20, a = 1, b = 0.1, g = 20, c = 1, d = 0.1, \xi = 0.01$, the initial value of the system $Y_0 = (x_0, y_0, z_0) = (0, 0, 0)$, the simulation step is 0.01, the simulation time is t , and the unit is second, $t \in (0, 40000)$. The 3D phase diagram of the system (6) and its projections are shown in Fig. 3. The red curve is a phase diagram in three dimensions, and the color map is its projections on three coordinate planes. It can be seen from the figure that the system can form a novel attractor with a certain shape by self-excitation even under zero initial condition Y_0 , which is different from other chaotic systems. Fig. 4 shows the time-domain waveform and power spectral density of the state variable x , respectively. Fig. 4 illustrates the state variable x meets the conditions of forming a chaotic attractor. Let's continue to analyze the nonlinear characteristics of the system (6) in terms of the 0-1 test, Poincaré map, and the LEs. The graph of 0-1 test distribution in Fig. 5(a) is unbounded, which meets the condition of forming an attractor. Fig. 5(b) is the Poincaré map on $z - y$ plane when $x = 0$. The Poincaré map is composed of a dense set of points, showing that the system is chaotic. At this time, The LEs of the system is $LE_1 = 0.11475, LE_2 \approx 0, LE_3 = -11.7323$. In addition to having a zero LEs, there is also a positive and a negative LEs, and $\sum_{i=1}^3 LE_i < 0$, which further confirms that the system is chaotic.

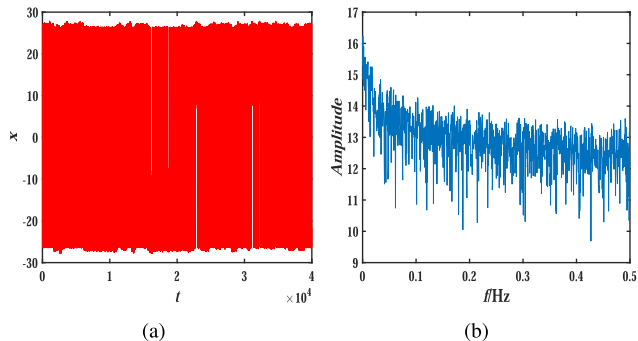


FIGURE 4. The time-domain waveform and power spectral density of variable x : (a) time-domain waveform; (b) power spectral density.

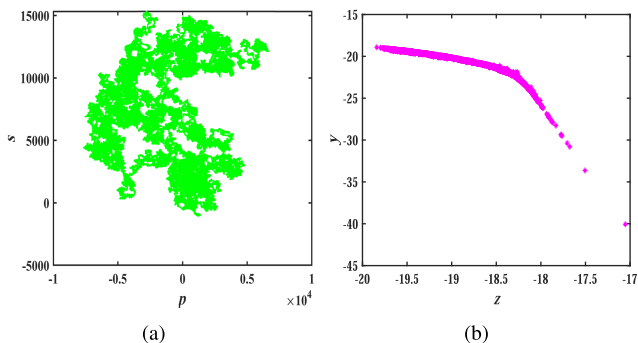


FIGURE 5. 0-1 test and Poincaré map of the system (6): (a) 0-1 test distribution; (b) Poincaré map.

III. TRANSIENT TRANSITION BEHAVIORS

Transient chaos is a unique phenomenon in nonlinear systems, and it appears in many studies. However, these reports only show that some systems only have one or two transient processes or transient transition under certain parameters, and the existence of transients is not universal. This section will focus on the transient transition that exists over a wide range in the proposed system, and discuss the transient transition phenomena with the changes of the system parameters and the initial value.

A. TRANSIENT TRANSITION WHEN PARAMETERS CHANGE

To fully reflect the system's rich transient transition behavior, calculate the chaotic characteristic diagram of the system (6). We fixed parameters $a = c = 1, b = d = 0.1, \xi = 0.01$, changed e and g , let $e \in (0, 50), g \in (0, 50)$, set the initial value $Y_0 = (0, 0, 0)$, and the simulation time $t = 2000$ seconds. Fig. 6 shows the chaotic characteristic diagram of the Largest Lyapunov exponent (LLE) as a function of the system parameters e and g . From the color distribution in Fig. 6, it can be seen that the LLE values of the system are different under the change of e and g , which reflects the law of LLE increasing values with the increase of parameters e and g . This means that for different values of e and g , their LEs are quite different.

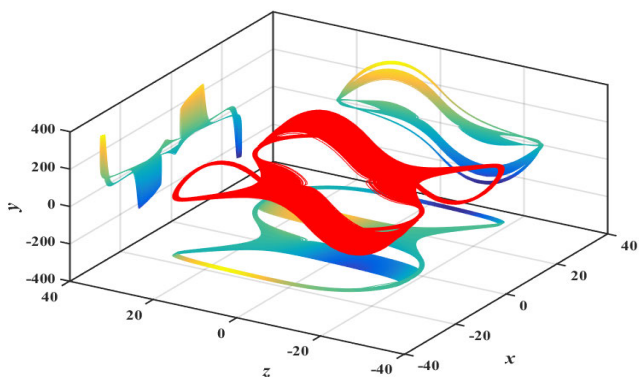


FIGURE 3. 3D-phase diagram and its projections of the system (6).

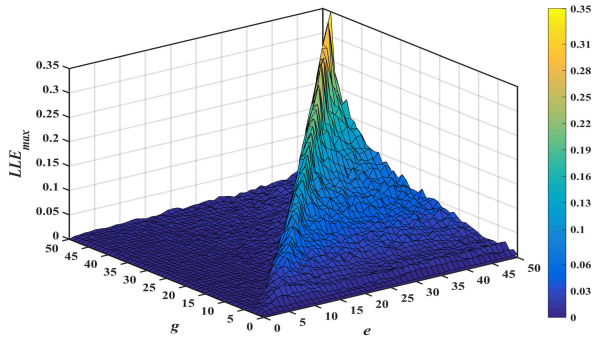


FIGURE 6. The 3D chaotic characteristic diagram of the system (6), $a = c = 1, b = d = 0.1, Y_0 = (0, 0, 0), \xi = 0.01, e \in (0, 50), g \in (0, 50)$.

In the chaotic characteristic diagram, all colors are the ones with LLE greater than or equal to zero, which indicates that the initial state of the system is chaotic, and there are quasi-periodic and periodic behaviors under certain values of e and g . Therefore, when discussing the LEs, the judgment of the positive and negative of $LLE_i (i = 1, 2, 3)$ is only meaningful when the e and g is determined. More importantly, this LLE trend with parameters also implies that the system (6) may have rich dynamic behaviors. To compare the initial state and the stable state of the system, in our work, let $t \in (0, 2000)$ as the system's initial state, and $t \in (3.9 \times 10^4, 4 \times 10^4)$ is the system stable state.

In Section III-A, it is assumed that the initial value of the system $Y_0 = (0, 0, 0)$. Different values e and g correspond to different values of the system. The i th

system parameter combination is recorded as $Y_{egi} = (e, g), (i = 1, 2, \dots, N)$, where N is a positive integer and represents the number of different parameter values of the system. The following will describe 6 typical transient behaviors for $Y_{egi} = (e, g), (i = 1, 2, \dots, 6)$. The phase diagram, dynamic behavior, and LEs and other parameters under different parameters are plotted in Table 1. Fig. 7 displays the projection of the phase diagram under different parameters on the $y - z$ plane. It can be observed from Table 1 and Fig. 7 that the projections of initial and stable states are different under various parameter combinations. Specifically, under the conditions of Y_{eg2} and Y_{eg4} , the system exhibits the initial chaos to the stable quasi-periodic; both Y_{eg1} and Y_{eg3} show that the initial state is a quasi-period, and the stable state is another quasi-period that is different from the initial state; for Y_{eg5} , the attractor undergoes from a chaos to a periodic limit cycle; for Y_{eg6} , the attractor moves from a quasi-periodic to a stable periodic state.

Only the six combinations of parameter values are discussed here due to the limitation of the length of the article. The method of spectral entropy SE will be used in the following to demonstrate that there are still rich transient behaviors for other parameters. The above analysis fully shows that during the process of parameter changes, the system has rich transient forms, which has never been reported in previous literature.

B. TRANSIENT TRANSITION WHEN THE INITIAL CHANGE

To discuss the rich transient behavior when the initial value of the system changes, it is necessary to compare the initial state with a stable state. In this section, the simulation time

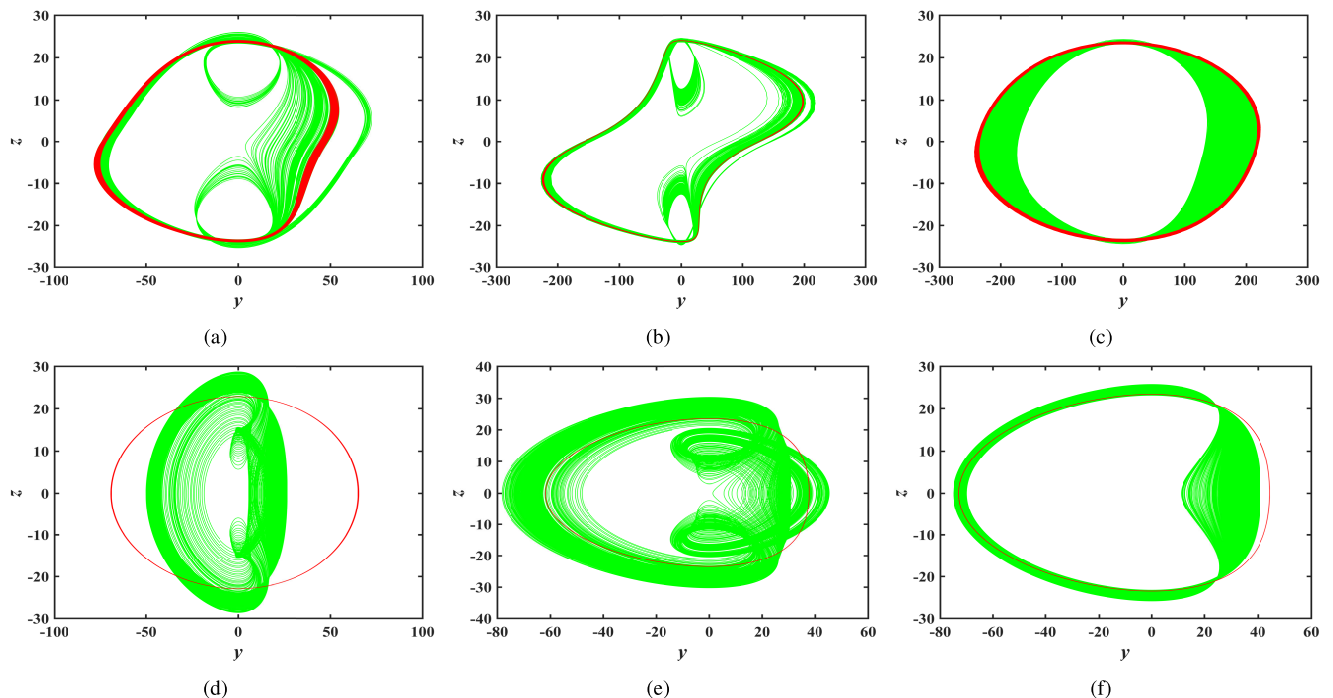


FIGURE 7. Phase diagrams of attractor projection on the $y - z$ plane for initial and stable states under $a = c = 1, b = d = 0.1, \xi = 0.01, Y_0 = (0, 0, 0)$, and different $Y_{egi} = (e, g), (i = 1, 2, \dots, 6)$: (a) Y_{eg1} ; (b) Y_{eg2} ; (c) Y_{eg3} ; (d) Y_{eg4} ; (e) Y_{eg5} ; (f) Y_{eg6} .

TABLE 1. System status under different $Y_{egi} = (e, g), (i = 1, 2, \dots, 6)$.

Y_{egi}	(e, g)	Status	LEs	Color	Phase diagram
Y_{eg1}	(4.5, 1.5)	initial:quasi-periodic stable:quasi-periodic	0, 0, -0.71665 0, 0, -0.74617	green red	Fig. 7(a)
Y_{eg2}	(16, 15)	initial:chaos stable:quasi-periodic	0.16919, -0.14080, -8.74361 0, 0, -8.43071	green red	Fig. 7(b)
Y_{eg3}	(45, 1.5)	initial:quasi-periodic stable:quasi-periodic	0, 0, -0.74940 0, 0, -0.74850	green red	Fig. 7(c)
Y_{eg4}	(1, 0.01)	initial:chaos stable:quasi-periodic	0.00617, 0, -0.01120 0, 0, -0.00533	green red	Fig. 7(d)
Y_{eg5}	(3, 0.01)	initial:chaos stable:periodic	0.01301, 0, -0.01931 0, -0.00159, -0.00565	green red	Fig. 7(e)
Y_{eg6}	(5, 0.01)	initial:quasi-periodic stable:periodic	0, 0, -0.00873 0, -0.00159, -0.00547	green red	Fig. 7(f)

$t = 2000$ seconds and $t = 4 \times 10^4$ seconds were chosen as the initial state and stable state, respectively. When fixing $e = 1, a = c = 1, g = 0.1, b = d = 0.1, \xi = 0.01$, and varying initial value $Y_0 = (x_0, y_0, 2x_0)$, where $x_0 \in (-50, 50)$ and $y_0 \in (-50, 50)$, Fig. 8 shows the dynamic behavior of the initial and stable state.

The color distribution in Fig. 8(a) indicates that the initial state of the system is mostly chaotic and quasi-periodic, and the shape of color distribution shows a certain regularity. It is odd symmetrical in general. At the same time, in addition to a small strip-shaped area near the center, the color points representing the quasi-periodic state are mainly regularly distributed in two triangular areas where the absolute values of coordinate (x_0, y_0) are large. Such distribution characteristics also suggest that there may be symmetrical attractors in the initial state of the system. Fig. 8(b) shows that the stable state of the system is a quasi-periodic behavior. Comparing Fig. 8(a) and (b), it can be seen that the corresponding position of the color distribution region representing the chaos in Fig. 8(a) changes into a quasi-periodic state in Fig. 8(b), indicating that the system has a lot of transient behaviors. It should be noted that although the quasi-periodic region in Fig. 8(a) still the quasi-periodic state in the corresponding area in Fig. 8(b), this does not mean that there is no transient behavior, and they are maybe two different quasi-periodic attractors. The same is true for the transient process from chaos to a quasi-periodic state. The different chaotic attractors in Fig. 8(a) may correspond to the same quasi-periodic attractor in the stable state.

In order to further investigate the transient behavior when the initial value changes $Y0_i = (x_0, y_0, 2x_0), (i = 1, 2, \dots, 10)$, the initial values, phase diagram color, states, and LEs are plotted in Table 2. According to the parameters in Table 2, the phase diagram of the system projected on the $y - z$ plane is shown in Fig. 9.

Fig. 9(a) shows the phase diagrams of the initial values $Y0_1$ and $Y0_2$ respectively, and Fig. 9(b) corresponds to the phase diagrams of the initial values $Y0_3$ and $Y0_4$ respectively. It can be seen from Fig. 9(a) and (b) that the shape attractors

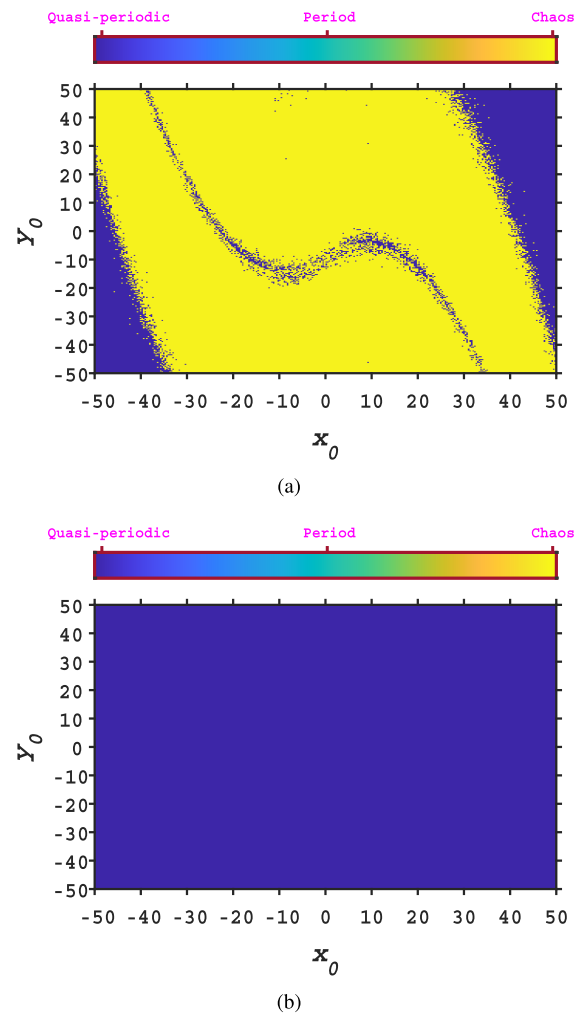


FIGURE 8. Dynamic behavior diagram of the system (6) for $Y_0 = (x_0, y_0, 2x_0)$, where $x_0 \in (-50, 50)$, and $y_0 \in (-50, 50)$: (a) initial state; (b) stable state.

are symmetrical at the initial state, and the stable states are quasi-periodic attractors, which is consistent with the color distribution of the dynamic behavior diagram of Fig. 8.

TABLE 2. System status under different $Y0_i = (x_0, y_0, 2x_0)$, ($i = 1, 2, \dots, 10$).

$Y0_i$	$(x_0, y_0, 2x_0)$	Status	LEs	Color	Phase diagram
$Y0_1$	$(4.5, -15.5, 9)$	initial:chaos stable:quasi-periodic	0.02314, -0.01693, -0.05599 0, 0, -0.05072	green blue	Fig. 9(a)
$Y0_2$	$(-5, -3, -10)$	initial:chaos stable:quasi-periodic	0.02194, -0.01988, -0.05002 0, 0, -0.05043	cyan red	
$Y0_3$	$(-15, -15, -30)$	initial:chaos stable:quasi-periodic	0.01390, -0.02065, -0.04892 0, 0, -0.05045	green blue	Fig. 9(b)
$Y0_4$	$(12.5, -10^{-10}, 25)$	initial:chaos stable:quasi-periodic	0.01260, -0.01240, -0.05534 0, 0, -0.05068	cyan red	
$Y0_5$	$(4.5001, -15.5, 9.0002)$	initial:quasi-periodic stable:quasi-periodic	0, 0, -0.05077 0, 0, -0.04989	green red	Fig. 9(c)
$Y0_6$	$(10, -10^{-10}, 20)$	initial:quasi-periodic stable:quasi-periodic	0, 0, -0.05403 0, 0, -0.05010	green red	Fig. 9(d)
$Y0_7$	$(0.5, -5, 1)$	initial:chaos stable:quasi-periodic	0.01152, -0.01900, -0.04725 0, 0, -0.05030	blue red	Fig. 9(e)
$Y0_8$	$(4, -5, 8)$	initial:chaos stable:quasi-periodic	0.01429, -0.01506, -0.05314 0, 0, -0.05063	blue red	Fig. 9(f)
$Y0_9$	$(5, -5, 10)$	initial:chaos stable:quasi-periodic	0.01483, -0.01527, -0.04447 0, 0, -0.05045	blue red	Fig. 9(g)
$Y0_{10}$	$(5, -3, 10)$	initial:chaos stable:quasi-periodic	0.01009, -0.01569, -0.05024 0, 0, -0.05051	blue red	Fig. 9(h)

Combined with table 2, we could find that the initial state has symmetric chaotic attractors for $Y0_1$ and $Y0_2$, but has completely different quasi-periodic limit cycles in the stable state; when the initial values are $Y0_3$ and $Y0_4$, the initial state shows symmetric chaotic attractors, but the stable state shows the same shape of the quasi-periodic limit cycle. This indicates that the system is sensitive to the change of the initial value, and the transient phenomenon is very complex.

The phase diagrams corresponding to the initial values $Y0_5$ and $Y0_6$ are shown in Fig. 9(c) and (d), respectively. The phase diagrams under these two initial values have in common that the initial state is a quasi-periodic attractor, while the stable state is another quasi-periodic limit cycle different from the initial state. It shows that under different initial conditions, the state of the system can transit from one quasi-periodic state to another quasi-periodic state shown in Fig. 8.

Table 2 shows that for four different initial values $Y0_i$, ($i = 7, 8, 9, 10$), the initial states are chaotic, and the stable states are quasi-periodic. Fig. 9(e)-(h) are phase diagrams corresponding to these different initial values. The phase diagrams reveal that under these four initial values, the initial states are different chaotic attractors, but the stable state coincides with the same shape of the quasi-periodic limit cycle. This confirms the hypothesis mentioned earlier does exist, that is, different chaotic attractor regions can evolve into the same quasi-periodic attractor.

In summary, it was found that during the change of the initial value, the initial state of the system includes symmetric attractors, different states of quasi-periodic limit cycles, and

different hidden chaotic attractors. However, there are few types of quasi-periodic attractors displayed in the stable state. This is because the dynamic behavior of the memristive system is more sensitive to the initial value, which makes the transient transition behavior induced by the change of the initial more abundant. On the other hand, it shows that the transition behaviors displayed are different under different initial values, suggesting that the system has complex transient transition behavior. Such a rich and complex transient behavior has never been reported in the existing literature.

IV. ANALYSIS OF MULTIPLE TRANSIENT TRANSITION BEHAVIOR

In the above analysis, the chaos characteristic diagram and phase diagram are used to show that the transient transition behavior of the system is universal from the perspective of changing the parameter or initial value. However, there is no detailed study on the evolution from the initial state to the stable state. In this section, several specific examples are given to illustrate the process of the transient transition behavior, and multiple transient transitions phenomena are identified for the new memristive system.

A. TRANSITION FROM CHAOTIC STATE TO PERIODIC STATE

Set the system parameters $e = 4$, $a = 1$, $b = 0.1$, $g = 0.001$, $c = 1$, $d = 0.1$, $\xi = 0.01$, the initial value $Y_0 = (x_0, y_0, z_0) = (0, 0, 0)$, the simulation parameters simulation step is 0.01, and the simulation time $t \in (0, 40000)$. The time-domain wave and phase diagram of the state variable y are shown in Fig. 10. When $t \in (0, 2871)$ shown in Fig. 10(a),

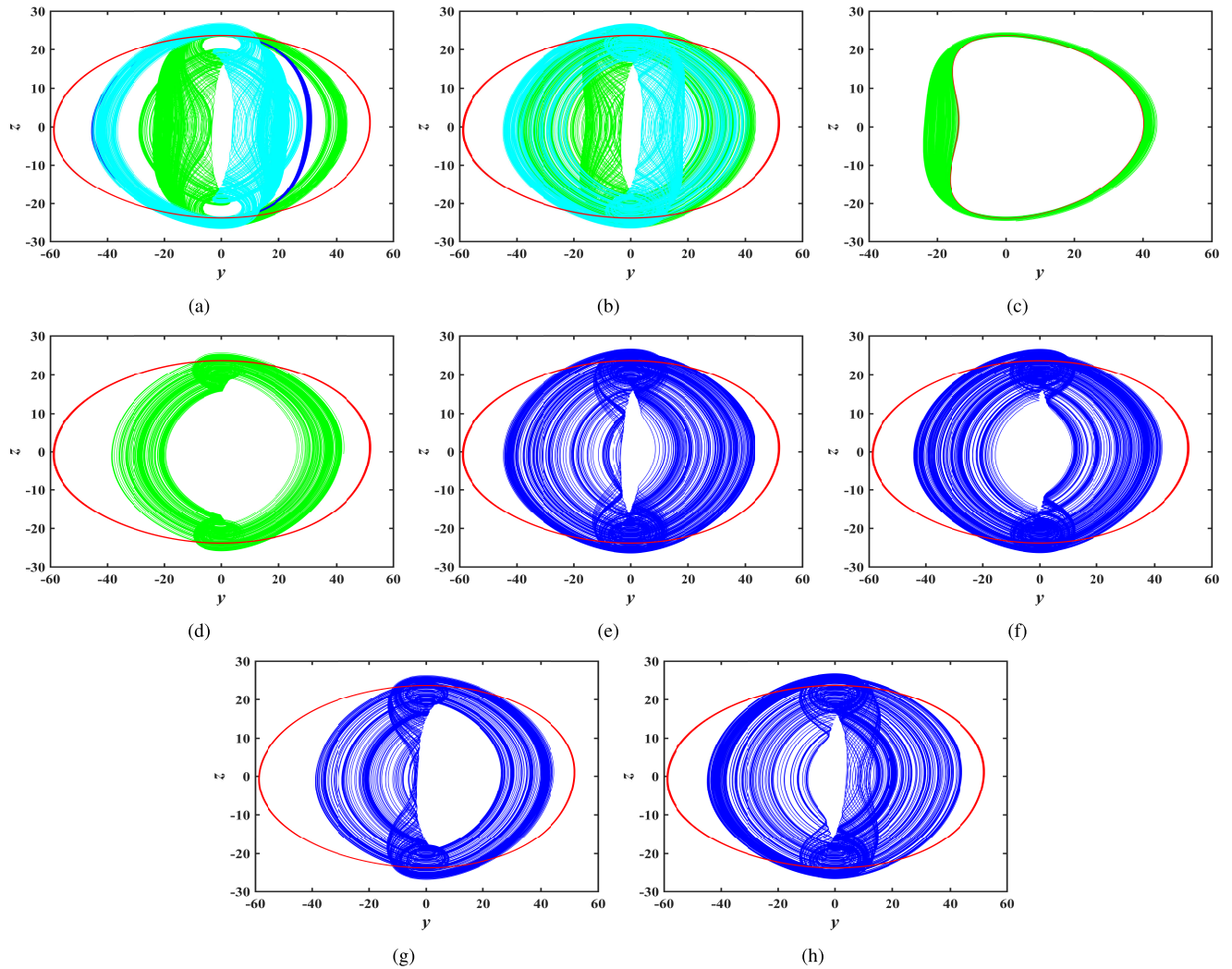


FIGURE 9. Phase diagrams of attractor projection on the $y - z$ plane for initial and stable states under $e = 1, a = c = 1, b = d = 0.1, g = 0.1, \xi = 0.01$, and different $Y_0 = (x_0, y_0, 2x_0)$, where $x_0 \in (-50, 50), y_0 \in (-50, 50)$: (a) Y_{01} and Y_{02} ; (b) Y_{03} and Y_{04} ; (c) Y_{05} ; (d) Y_{06} ; (e) Y_{07} ; (f) Y_{08} ; (g) Y_{09} ; (h) Y_{10} .

the time-domain wave is aperiodic. At this time, $LE_1 = 0.0037436, LE_2 \approx 0$, and $LE_3 = -0.0046961$, so the system is chaotic during this period; when $t \in (2871, 40000)$, the time-domain wave displays a clear periodicity. Therefore, the transient transition occurs, and the $y - z$ plane phase diagram in Fig. 10(b) also shows the corresponding transient transition state.

B. THREE TRANSITION STATES

Only change the system simulation initial value, let $Y_0 = (x_0, y_0, z_0) = (-1, -5, -10)$, keep the other system and simulation parameters used in Section IV-A unchanged. Continue to do the simulation about the time-domain wave and phase diagram of variable y , as shown in Fig. 11. Fig. 11(a) indicates that the time-domain waveform is divided into three stages. Specifically, the curve marked in blue has no periodicity, when $t \in (0, 1200)$; the red gradually changes from disorder to order when $t \in (1200, 8331)$; the magenta changes

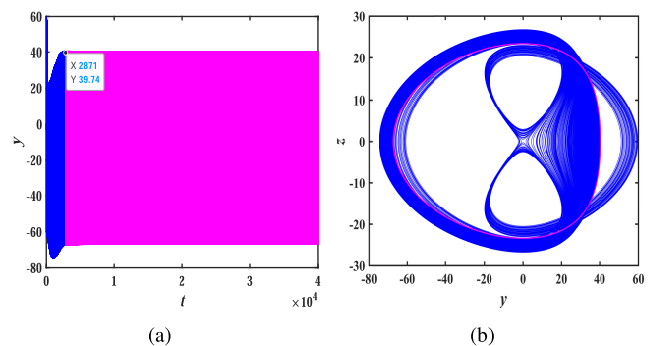


FIGURE 10. The time-domain waveform and phase diagram of variable y , blue ($t \in (0, 2871)$), magenta ($t \in (2871, 40000)$): (a) time-domain waveform; (b) phase diagram.

regularly when $t \in (8331, 40000)$. The phase diagrams on the $y - z$ plane corresponding to the three stages are shown in Fig. 11(b), (c), and (d), respectively. As shown

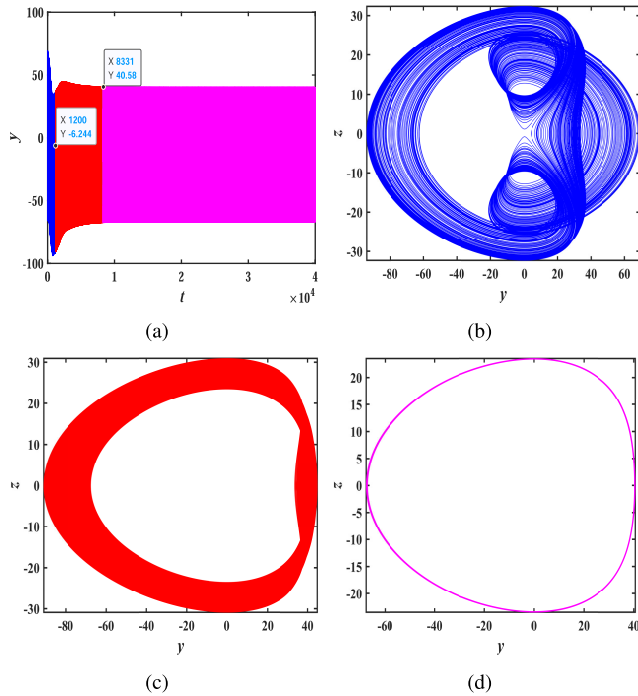


FIGURE 11. The time-domain waveform and phase diagram of variable y , blue ($t \in (0, 1200)$), red($t \in (1200, 8331)$), magenta ($t \in (8331, 40000)$): (a) time-domain waveform; (b) phase diagram ($t \in (0, 1200)$); (c) phase diagram ($t \in (1200, 8331)$); (d) phase diagram ($t \in (8331, 40000)$).

in Fig. 11(b), a strange attractor with a specific shape is formed during $t \in (0, 1200)$. During this period, $LE_1 = 0.0070777$, $LE_2 \approx 0$, $LE_3 = -0.0078112$, and the system behaves as a chaotic state. When $t \in (1200, 8331)$, $LE_1 = 0.0017679$, $LE_2 \approx 0$, $LE_3 = -0.0016252$. It seems like that the LEs satisfies to the characteristics of chaos and can form attractors. However, due to $\sum_{i=1}^3 LE_i > 0$, the system is in an unstable state, as shown in Fig. 11(c). In the range of $t \in (8331, 40000)$, the time-domain wave shows obvious periodicity. And because $\sum_{i=1}^3 LE_i < 0$, at this time, the system is in a stable limit cycle state shown in Fig. 11(d).

It can be seen that under the above parameters, the system (6) transits from a chaotic state to an unstable two-dimensional torus, and finally stabilizes in the periodic state. There are three states from the beginning to the stable state, which is different from the transient transition behaviors reported in the existing data. This study reveals for the first time that the number of transition states could be equal to three.

C. FOUR TRANSITION STATES

Now, the transient transition process is studied from the perspective of two variables. When the system parameters are $e = 1$, $a = 1$, $b = 0.1$, $g = 0.1$, $c = 1$, $d = 0.1$, $\xi = 0.01$, the initial value of the system $Y_0 = (x_0, y_0, z_0) = (-1.5, 10.5, -3)$, the simulation step

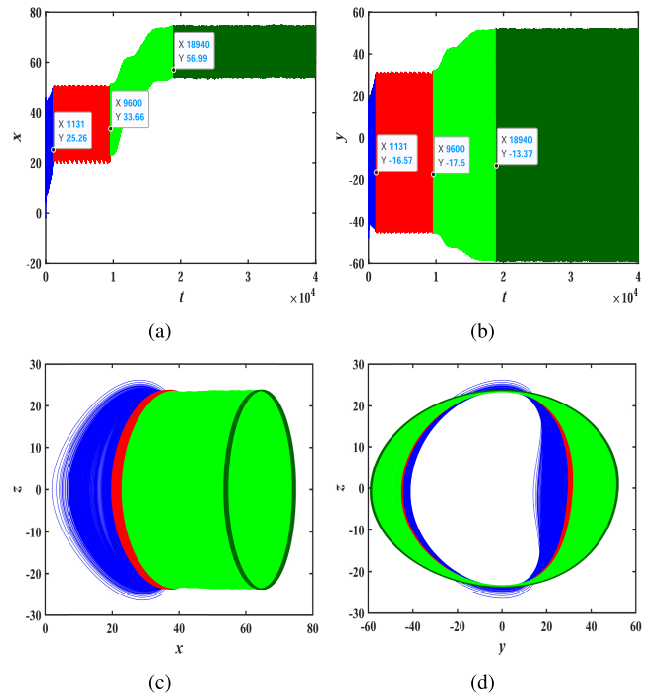


FIGURE 12. The time-domain waveform and phase diagram of variables, blue ($t \in (0, 1131)$), red($t \in (1131, 9600)$), green ($t \in (9600, 18940)$), dark green ($t \in (18940, 40000)$): (a) time-domain waveform of x ; (b) time-domain waveform of y ; (c) phase diagram on $x - z$; (d) phase diagram on $y - z$.

is 0.01, and the simulation time $t \in (0, 40000)$, the time-domain waves of the state variable x and y are shown in Fig. 12 (a) and (b). In the four-time periods of $t \in (0, 1131)$, $t \in (1131, 9600)$, $t \in (9600, 18940)$, and $t \in (18940, 40000)$, the time-domain waveform of the system has different changing rules, which determines that the system is in different states in these periods. In the time-domain waveform diagrams, the blue, red, green, and dark green curves are used to correspond to these four-time periods, respectively, and the same is true for the phase diagrams 12(c) and (d). When $t \in (0, 1131)$, $LE_1 = 0.0056637$, $LE_2 = -0.0040208$, $LE_3 = -0.048771$, and $\sum_{i=1}^3 LE_i < 0$, observing the time-domain waveform and phase diagram, we can see that the initial state of the system is similar to a two-dimensional torus. When $t \in (1131, 9600)$ the time-domain wave reflects the quasi-periodic change. At this time, $LE_1 = LE_2 \approx 0$, $LE_3 = -0.049328$, the system is in a quasi-periodic limit cycle state. When $t \in (9600, 18940)$, it can be seen from the time-domain wave that the absolute value of the state variable increases significantly to a bounded value as time increases. Combined with the phase diagram, we find that the attractor formed at this time is a bounded two-dimensional torus. When $t \in (18940, 40000)$, both the time-domain waveform and the phase diagram show that the system was in a quasi-period limit cycle. Due to the obvious time-domain boundary of the variable, the system experienced two different transient processes from the initial to the

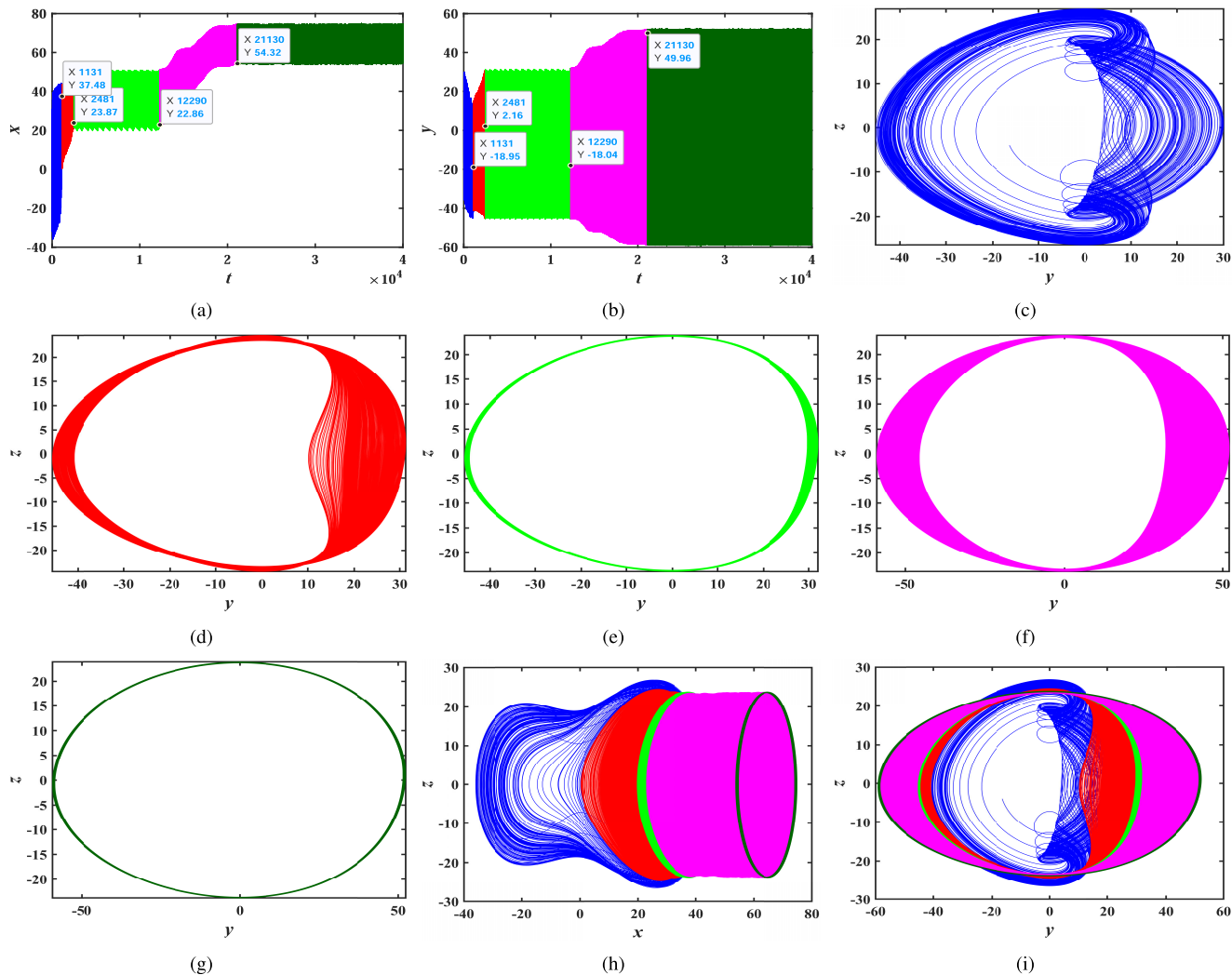


FIGURE 13. The time-domain waveform and phase diagram of variables, blue ($t \in (0, 1131)$), red ($t \in (1131, 2481)$), green ($t \in (2481, 12290)$), magenta ($t \in (12290, 21130)$), dark green ($t \in (21130, 40000)$): (a) time-domain waveform of x ; (b) time-domain waveform of y ; (c) phase diagram on $y - z$, $t \in (0, 1131)$; (d) phase diagram on $y - z$, $t \in (1131, 2481)$; (e) phase diagram on $y - z$, $t \in (2481, 12290)$; (f) phase diagram on $y - z$, $t \in (12290, 21130)$; (g) phase diagram on $y - z$, $t \in (21130, 40000)$; (h) phase diagram on $x - z$, $t \in (0, 40000)$; (i) phase diagram on $y - z$, $t \in (0, 40000)$.

stable state. This makes the process of system evolution more complicated and brings challenges to better understanding of memristive systems.

D. FIVE TRANSITION STATES

Under the parameters of Section IV-C, change the initial value $Y_0 = (x_0, y_0, z_0) = (0, 0, 0)$, and continue to study the transient transition state of the system (6) through the time-domain waveform and phase diagram of two variables. The time-domain diagrams of the state variables x and y are shown in Fig. 13(a) and (b). The time-domain waveforms point out that there are five-time period boundaries $t \in (0, 1131)$, $t \in (1131, 2481)$, $t \in (2481, 12290)$, $t \in (12290, 21130)$, and $t \in (21130, 40000)$, which means that the system has five different transient transition states. In Fig. 13, the time-domain waveforms and two-dimensional phase diagrams of the five-time periods are represented by blue, red, green,

magenta, and dark green, respectively. When $t \in (0, 1131)$, at this time, $LE_1 = 0.0066518$, $LE_2 \approx 0$, $LE_3 = -0.056851$, combined with Fig. 13(c), it can be seen that the initial state of the system is chaotic. When $t \in (1131, 2481)$, $LE_1 = 0.0077506$, $LE_2 = -0.0046288$, $LE_3 = -0.051616$, and $\sum_{i=1}^3 LE_i < 0$, there is a positive LEs, so the system can form a bounded attractor. Fig. 13(d) also shows that the system attractor is a two-dimensional torus at this time. When $t \in (2481, 12290)$, it can be seen that the variable has a certain periodicity on the time-domain diagram, and the phase diagram in Fig. 13(e) shows that the system is in a quasi-periodic state. When $t \in (12290, 21130)$, there is a positive LEs, and the phase diagram Fig. 13(f) shows that the attractor is in a bounded two-dimensional torus. When $t \in (21130, 40000)$, the time-domain waveform is periodic, and Fig. 13(g) indicates that the system is in the quasi-periodic limit cycle state.

The projection phase diagram on $x - z$ and $y - z$ plane during the whole time, $t \in (0, 40000)$, is shown in Fig. 13(h) and (i) where, fully reflects the complex process of the transient transition behaviors. Compared with the situation described in Section IV-C, under the new initial conditions, a chaotic state is added to the initial state. It shows that the nonlinear dynamic characteristics of the system (6) are very complicated. There are another three transient processes from the initial state to the stable state. Such a variety of transient states greatly increases the complexity of the system and provides more options for the engineering application of memristors.

To sum it up, this section mainly describes the transition state behavior of the system from the initial state to a stable state with several examples. The evolution of time-domain waveforms about variables and attractor phase diagrams are given in detail. It is worth pointing out that there are innumerable types of transition behaviors, which will not be fully studied here. This section reveals for the first time the existence of multiple transient transitions behavior. These studies will bring a lot of new thinking about the theory and application of memristors in circuit research.

V. MULTISTABILITY STATE

Under the same system parameters and different initial values, the system has a different stable state, which can reflect the existence of a multistability state. Going back to the examples given at the 3 Section, we know that when the system parameters are $e = 1, a = 1, b = 0.1, g = 0.1, c = 1, d = 0.1, \xi = 0.01$, the initial value $Y_0 = (x_0, y_0, 2x_0), x_0 \in (-50, 50), y_0 \in (-50, 50)$. Specifically, the initial value $Y_{0i}, (i = 1, 2, 5)$, The stable state of the system has attractors with different shapes, so it is proved that the system has a multistability state phenomenon.

VI. COMPLEXITY ANALYSIS

In this section, SE algorithm [52], [77] which can describe the global complexity of the system is used to analyze the system. Fixed system parameters, $a = 1, b = 0.1, g = 0.1, c = 1, d = 0.1, \xi = 0.01$. Fig. 14 shows the changes of

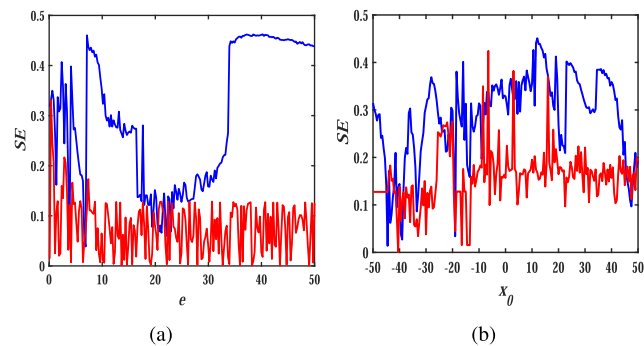


FIGURE 14. SE varies with parameters and initial values, blue (initial), red(stable): (a) $Y_0 = (0, 0, 0), e \in (0, 50)$; (b) $e = 1, Y_0 = (x_0, x_0, 2x_0), x_0 \in (-50, 50)$.

SE with system parameters e and initial value, respectively. Fig. 14 compares the SE change between the initial and stable state. The blue curve represents the simulation time is 2000 seconds, which represents the initial state of the system; the red curve represents the simulation time is 40000 seconds, which represents the stable state of the system.

In Fig. 14(a), the system initial value $Y_0 = (0, 0, 0)$, SE is a function that changes with the system parameter e . In the range of $e \in (0, 50)$, except for a few values, the red curve is mostly located below the blue, indicating that the complexity in the stable state is less than the initial state. The transition of complexity from high to low reveals that there must be some transition states during parameter changes. SE is a function that changes with the system's initial value $Y_0 = (x_0, x_0, 2x_0), x_0 \in (-50, 50)$ illustrated in Fig. 14(b), where the SE fluctuates greatly, reflecting that the system is sensitive to the initial value. At the same time, the blue curve is always above the red curve, reflecting the different complexity of the initial and final states, which also reflects that the system has a transition state behavior when the initial value changes. From the high complexity of the initial state to the low complexity of the stable state, it can be inferred that the system transitioned from a chaotic or a high-density two-dimensional torus state to a quasi-periodic limit cycle or periodic state, which is consistent with the previous analysis results. It further confirms that the system generally has a transition state behavior.

VII. CIRCUIT DESIGN

In this section, the specific circuit is designed for the system in which there are five transition behaviors discussed in Section IV-D. Equation (13) can be obtained from (6), (7) and (8). According to the range of phase diagrams of numerical simulation, to realize the system through the ideal operational amplifier, it is necessary to use Equation (14) to carry out variable substitution. Substituting Equation (14) into (13) gives Equation (15).

$$\begin{cases} \frac{dx}{dt} = z \\ \frac{dy}{dt} = eW_{\varphi 1}(x)z + gW_{\varphi 2}(z)y + \xi \\ \frac{dz}{dt} = y \end{cases} \quad (13)$$

$$\begin{cases} x = 10x' \\ y = 10y' \\ z = 10z' \end{cases} \quad (14)$$

$$\begin{cases} \frac{dx'}{dt} = z' \\ \frac{dy'}{dt} = eW_{\varphi 1}(10x')z' + gW_{\varphi 2}(10z')y' + 0.1\xi \\ \frac{dz'}{dt} = y' \end{cases} \quad (15)$$

Designing the circuit equation corresponding to Equation (15), we could get Equation (16), where RC is the

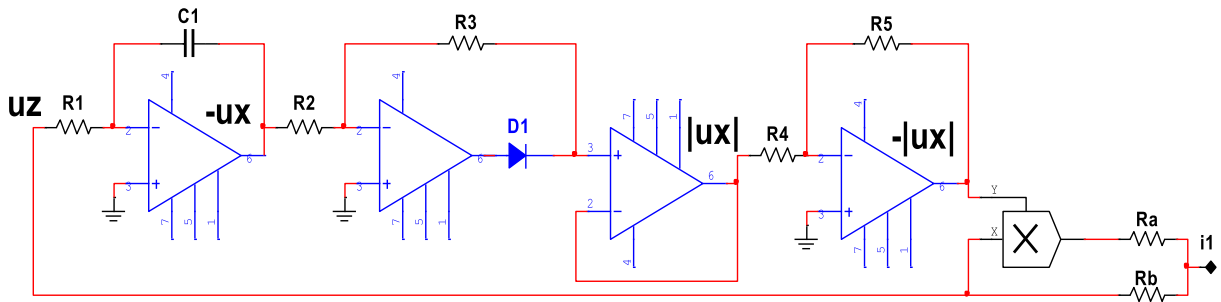


FIGURE 15. The circuit schematic of the memristor unit $W_1'(u_x) u_z$.

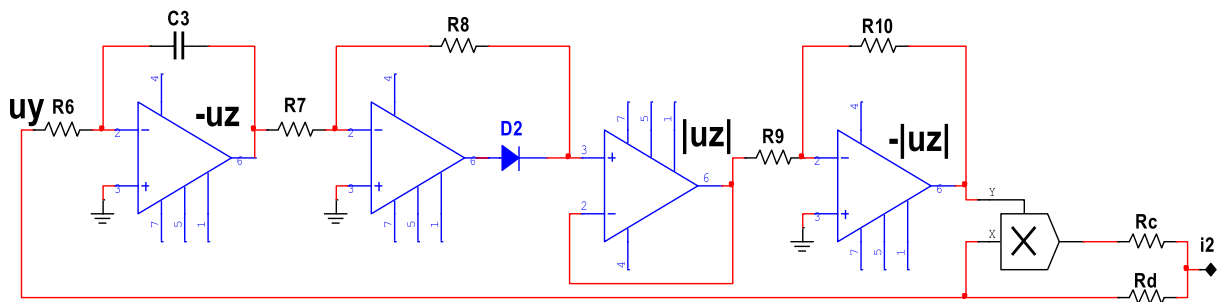


FIGURE 16. The circuit schematic of the memristor unit $W_2'(u_z) u_y$.

system time constant.

$$\begin{cases} RC \frac{du_x}{dt} = u_z \\ RC \frac{du_y}{dt} = eW_{\varphi 1}(10u_x) u_z + gW_{\varphi 2}(10u_z) u_y + 0.1\xi \\ RC \frac{du_z}{dt} = u_y \end{cases} \quad (16)$$

In the circuit equation of (16), set the parameters $e = 1$, $a = 1$, $b = 0.1$, $g = 0.1$, $c = 1$, $d = 0.1$, $\xi = 0.01$. To complete the system circuit, the memristor model unit must be designed first. From (16), there is

$$\begin{cases} W_1'(u_x) = eW_{\varphi 1}(10u_x) = ea - 10eb |u_x| \\ W_2'(u_z) = gW_{\varphi 2}(10u_z) = gc - 10gd |u_z| \end{cases} \quad (17)$$

Performing the substitution of the parameter values, we have

$$\begin{cases} W_1'(u_x) = ea - 10eb |u_x| = 1 - |u_x| \\ W_2'(u_z) = gc - 10gd |u_z| = 0.1 - 0.1 |u_z| \end{cases} \quad (18)$$

Then the circuit of the memristor unit $W_1'(u_x) u_z$ could be obtained in Fig. 15.

Assume that the time constant $\tau = RC$, take $R = 10k\Omega$, then $C_1 = C = 33nF$. In the circuit schematic of Fig. 15, absolute value circuit $R_2 = R_3 = 200k\Omega$, TL082 is used in op-amp, the multiplier uses AD633, the model of the diode D1 is 1N4148, $R_4 = R_5 = 10k\Omega$, the gain of multiplier $g_1 = 1$.

Then the memristive circuit equation will be

$$\begin{cases} i = R \left(\frac{u_z}{R_b} - \frac{g_1}{R_a} |u_x| u_z \right) = R \left(\frac{1}{R_b} - \frac{g_1}{R_a} |u_x| \right) u_z \\ RC \frac{du_x}{dt} = u_z \end{cases} \quad (19)$$

So there are $\frac{R}{R_b} = ea = 1$, $\frac{Rg_1}{R_a} = 10eb = 1$, we could get $R_a = R_b = 10k\Omega$. The above completes the circuit design of $W_1'(u_x) u_z$. Similarly, the circuit of the memristor unit $W_2'(u_z) u_y$ is shown in Fig. 16.

In Fig. 16, $R_6 = 10k\Omega$, $C_3 = C = 33nF$, $R_7 = R_8 = 200k\Omega$, the op-amp uses TL082, the multiplier uses AD633, the diode type is 1N4148, $R_9 = R_{10} = 10k\Omega$, the multiplier gain $g_2 = 1$. So the memristive circuit equation is

$$\begin{cases} i = R \left(\frac{u_y}{R_d} - \frac{g_2}{R_c} |u_z| u_y \right) = R \left(\frac{1}{R_d} - \frac{g_2}{R_c} |u_z| \right) u_y \\ RC \frac{du_z}{dt} = u_y \end{cases} \quad (20)$$

where $\frac{R}{R_d} = gc = 0.1$, $\frac{Rg_2}{R_c} = 10gd = 0.1$, and $R_c = R_d = 100k\Omega$.

The voltage signals u_y and u_z used in Fig. 15 and 16 are implemented by the inverter circuit shown in Fig. 17(a), where $R_{12} = R_{13} = 10k\Omega$, $C_2 = C_1 = C_3 = 33nF$, $R_{11} = 10k\Omega$, DC voltage $0.1\xi = 0.001V$. The current i_1 and i_2 which is shown in Fig. 17(b) are the current outputs of the memristor in Fig. 15 and Fig. 16, respectively.

The phase diagrams of the circuit system (16) are simulated by Multisim in Fig. 18. The power supply voltage of the circuit system is $\pm 15V$. The chaotic attractor shown

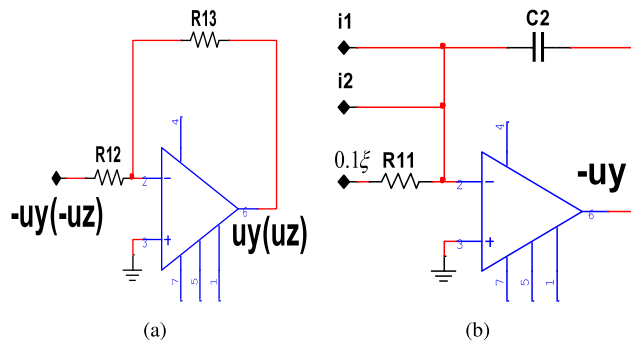


FIGURE 17. Inverter and overall circuit schematic: (a) inverter circuit; (b) overall connection.

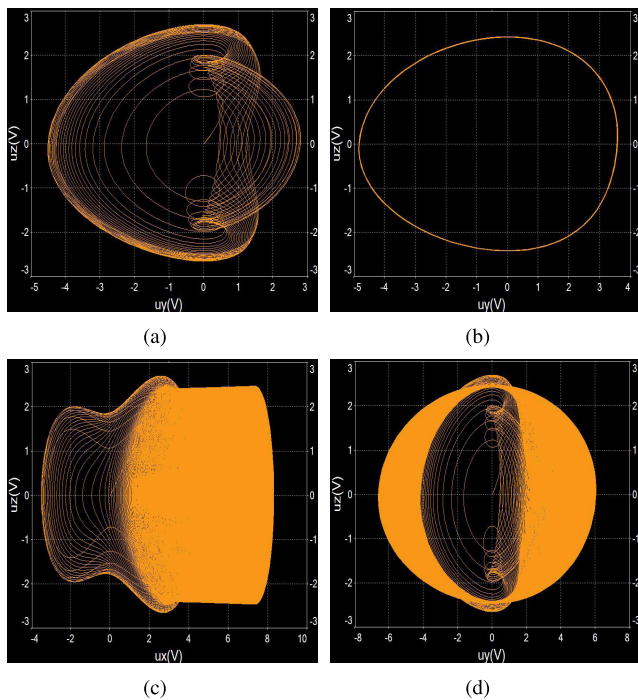


FIGURE 18. The phase diagrams of the circuit system (18): (a) the initial state on the $uy - uz$ plane; (b) the stable state on the $uy - uz$ plane; (c) the attractor on the $ux - uz$ plane; (d) the attractor on the $uy - uz$ plane.

in Fig. 18(a) is the initial state of the system on the $uy - uz$ plane, and Fig. 18(b) is its stable state. Fig. 18(c) and 18(d) show the phase diagram of the system (16) on the $ux - uz$ plane and the $uy - uz$ plane respectively. Compared with Fig. 18 and Fig. 13, it is found that the circuit simulation results are highly consistent with the numerical simulation. So the correctness of the numerical simulation results is verified, and the system can be realized using off-the-shelf components.

VIII. CONCLUSIONS

In this paper, two memristors are used to replace the two linear resistors of a simple integrating circuit to obtain a nonlinear system with hidden attractors. It is found that when the parameters or initial values of the new system change,

there are transient transition behaviors. From the perspective of the chaotic characteristic diagram, phase diagram, and complexity SE, it is confirmed that the system has a wide range of transient transition behaviors. The process of specific transient transition behaviors is also analyzed. We know that from the initial to the stable the system could include two kinds, three kinds, four kinds, and five different kinds of states. The system has multiple transient transitions behavior. At the same time, under different initial conditions, the new system also shows multistability. Finally, the memristor unit circuit and the hidden system nonlinear circuit are designed according to the specific parameters of the system. The circuit simulation results are consistent with the numerical simulation.

Through the research of this paper, we could find that if the memristor, a newly born component, is applied to a simple integrating circuit, it will produce complex nonlinear behaviors. This behavior is due to the non-linear nature of the memristor, which differs from linear elements. Numerical simulations were made to reveal the existence of multiple transient behaviors. However, the reasons (theoretical basis) why there is such a rich transient behavior for this memristive system, as well as other non-linear behaviors that are not reflected in this paper, are still worthy of future research and discussion.

ACKNOWLEDGMENT

The authors would like to thank the three anonymous reviewers for their constructive comments and insightful suggestions.

REFERENCES

- [1] F. Yu, Z. Zhang, L. Liu, H. Shen, Y. Huang, C. Shi, S. Cai, Y. Song, S. Du, and Q. Xu, "Secure communication scheme based on a new 5D multistable four-wing memristive hyperchaotic system with disturbance inputs," *Complexity*, vol. 2020, Jan. 2020, Art. no. 5859273.
- [2] S. Wang, Y. Cao, T. Huang, Y. Chen, P. Li, and S. Wen, "Sliding mode control of neural networks via continuous or periodic sampling event-triggering algorithm," *Neural Netw.*, vol. 121, pp. 140–147, Jan. 2020.
- [3] Y. V. Pershin and M. Di Ventra, "On the validity of memristor modeling in the neural network literature," *Neural Netw.*, vol. 121, pp. 52–56, Jan. 2020.
- [4] Y. Zhou, H. Q. Wu, B. Gao, W. Wu, Y. Xi, P. Yao, S. L. Zhang, Q. T. Zhang, and H. Qian, "Associative memory for image recovery with a high-performance memristor array," *Adv. Funct. Mater.*, vol. 29, no. 30, Jul. 2019, Art. no. 1900155.
- [5] L. Y. Xu, R. Yuan, Z. H. Zhu, K. Q. Liu, Z. K. Jing, Y. M. Cai, Y. Wang, Y. C. Yang, and R. Huang, "Memristor-based efficient in-memory logic for cryptologic and arithmetic applications," *Adv. Mater. Technol.*, vol. 4, no. 7, Jul. 2019, Art. no. 1900212.
- [6] M. Itoh and L. O. Chua, "Memristor oscillators," *Int. J. Bifurcation Chaos*, vol. 18, no. 11, pp. 3183–3206, Nov. 2008.
- [7] A. I. Ahamed and M. Lakshmanan, "Nonsmooth bifurcations, transient hyperchaos and hyperchaotic beats in a memristive Murali–Lakshmanan–Chua circuit," *Int. J. Bifurcation Chaos*, vol. 23, no. 6, Jun. 2013, Art. no. 1350098.
- [8] B. Bo-Cheng, L. Zhong, and X. Jian-Ping, "Transient chaos in smooth memristor oscillator," *Chin. Phys. B*, vol. 19, no. 3, Mar. 2010, Art. no. 030510.
- [9] H. Bao, T. Jiang, K. Chu, M. Chen, Q. Xu, and B. Bao, "Memristor-based canonical Chua's circuit: Extreme multistability in voltage-current domain and its controllability in flux-charge domain," *Complexity*, vol. 2018, Mar. 2018, Art. no. 5935637.

- [10] B. C. Bao, L. Xu, Z. M. Wu, M. Chen, and H. G. Wu, "Coexistence of multiple bifurcation modes in memristive diode-bridge-based canonical Chua's circuit," *Int. J. Electron.*, vol. 105, no. 7, pp. 1159–1169, 2018.
- [11] M. Chen, B. C. Bao, T. Jiang, H. Bao, Q. Xu, H. G. Wu, and J. Wang, "Flux-charge analysis of initial state-dependent dynamical behaviors of a memristor emulator-based Chua's circuit," *Int. J. Bifurcation Chaos*, vol. 28, no. 10, Sep. 2018, Art. no. 1850120.
- [12] B. C. Bao, H. G. Wu, L. Xu, M. Chen, and W. Hu, "Coexistence of multiple attractors in an active diode pair based Chua's circuit," *Int. J. Bifurcation Chaos*, vol. 28, no. 2, Feb. 2018, Art. no. 1850019.
- [13] M. Chen, J. J. Yu, Q. Yu, C. D. Li, and B. C. Bao, "A memristive diode bridge-based canonical Chua's circuit," *Entropy*, vol. 16, no. 12, pp. 6464–6476, Dec. 2014.
- [14] B. Bao, T. Jiang, G. Wang, P. Jin, H. Bao, and M. Chen, "Two-memristor-based Chua's hyperchaotic circuit with plane equilibrium and its extreme multistability," *Nonlinear Dyn.*, vol. 89, no. 2, pp. 1157–1171, Jul. 2017.
- [15] M. Chen, B.-C. Bao, and J. Yu, "Finding hidden attractors in improved memristor-based Chua's circuit," *Electron. Lett.*, vol. 51, no. 6, pp. 462–464, Mar. 2015.
- [16] H. Wu, Y. Ye, M. Chen, Q. Xu, and B. Bao, "Extremely slow passages in low-pass filter-based memristive oscillator," *Nonlinear Dyn.*, vol. 97, no. 4, pp. 2339–2353, Sep. 2019.
- [17] J. Luo, H. Bao, M. Chen, Q. Xu, and B. Bao, "Inductor-free multi-stable Chua's circuit constructed by improved PI-type memristor emulator and active Sallen–Key high-pass filter," *Eur. Phys. J. Special Topics*, vol. 228, no. 10, pp. 1983–1994, Oct. 2019.
- [18] Q. Xu, Q. Zhang, N. Wang, H. Wu, and B. Bao, "An improved memristive diode bridge-based band pass filter chaotic circuit," *Math. Problems Eng.*, vol. 2017, Oct. 2017, Art. no. 2461964.
- [19] B. Bao, N. Wang, Q. Xu, H. Wu, and Y. Hu, "A simple third-order memristive band pass filter chaotic circuit," *IEEE Trans. Circuits Syst. II, Exp. Briefs*, vol. 64, no. 8, pp. 977–981, Aug. 2017.
- [20] D. A. Prousalis, C. K. Volos, I. N. Stouboulos, and I. M. Kyprianidis, "Hyperchaotic memristive system with hidden attractors and its adaptive control scheme," *Nonlinear Dyn.*, vol. 90, no. 3, pp. 1681–1694, Nov. 2017.
- [21] R. Wang, M. Li, Z. Gao, and H. Sun, "A new memristor-based 5D chaotic system and circuit implementation," *Complexity*, vol. 2018, Dec. 2018, Art. no. 6069401.
- [22] B. A. Mezzatio, M. T. Motchongom, B. R. Wafo Tekam, R. Kengne, R. Tchitinga, and A. Fomethé, "A novel memristive 6D hyperchaotic autonomous system with hidden extreme multistability," *Chaos, Solitons Fractals*, vol. 120, pp. 100–115, Mar. 2019.
- [23] X. Hu, C. Liu, L. Liu, Y. Yao, and G. Zheng, "Multi-scroll hidden attractors and multi-wing hidden attractors in a 5-dimensional memristive system," *Chin. Phys. B*, vol. 26, no. 11, Oct. 2017, Art. no. 110502.
- [24] P. Saha, D. C. Saha, A. Ray, and A. R. Chowdhury, "Memristive non-linear system and hidden attractor," *Eur. Phys. J. Special Topics*, vol. 224, no. 8, pp. 1563–1574, Jul. 2015.
- [25] H. Bao, N. Wang, B. Bao, M. Chen, P. Jin, and G. Wang, "Initial condition-dependent dynamics and transient period in memristor-based hypogenetic jerk system with four line equilibria," *Commun. Nonlinear Sci. Numer. Simul.*, vol. 57, pp. 264–275, Apr. 2018.
- [26] B. Bao, N. Wang, M. Chen, Q. Xu, and J. Wang, "Inductor-free simplified Chua's circuit only using two-op-amp-based realization," *Nonlinear Dyn.*, vol. 84, no. 2, pp. 511–525, Apr. 2016.
- [27] Wu, Wang, Ju, Shen, and Zhou, "A nonvolatile fractional order memristor model and its complex dynamics," *Entropy*, vol. 21, no. 10, p. 955, 2019.
- [28] Y. Song, F. Yuan, and Y. Li, "Coexisting attractors and multistability in a simple memristive wien-bridge chaotic circuit," *Entropy*, vol. 21, no. 7, p. 678, 2019.
- [29] X. Zhong, M. Peng, M. Shahidehpour, and S. Guo, "Bifurcation and periodic solutions in memristive hyperchaotic system," *IEEE Access*, vol. 6, pp. 23202–23212, 2018.
- [30] M. Chen, M. X. Sun, B. C. Bao, H. G. Wu, Q. Xu, and J. Wang, "Controlling extreme multistability of memristor emulator-based dynamical circuit in flux–charge domain," *Nonlinear Dyn.*, vol. 91, no. 2, pp. 1395–1412, Jan. 2018.
- [31] B. C. Bao, P. Y. Wu, H. Bao, Q. Xu, and M. Chen, "Numerical and experimental confirmations of quasi-periodic behavior and chaotic bursting in third-order autonomous memristive oscillator," *Chaos, Solitons Fractals*, vol. 106, pp. 161–170, Jan. 2018.
- [32] H. Bao, B. C. Bao, Y. Lin, J. Wang, and H. G. Wu, "Hidden attractor and its dynamical characteristic in memristive self-oscillating system," *Acta Phys. Sinica*, vol. 65, no. 18, Sep. 2016, Art. no. 180501.
- [33] M. Chen, M. X. Sun, H. Bao, Y. H. Hu, and B. C. Bao, "Flux–charge analysis of two-memristor-based Chua's circuit: Dimensionality decreasing model for detecting extreme multistability," *IEEE Trans. Ind. Electron.*, vol. 67, no. 3, pp. 2197–2206, Mar. 2020.
- [34] H. Chang, Y. Li, F. Yuan, and G. Chen, "Extreme multistability with hidden attractors in a simplest memristor-based circuit," *Int. J. Bifurcation Chaos*, vol. 29, no. 06, Jun. 2019, Art. no. 1950086.
- [35] B. Bao, A. Hu, H. Bao, Q. Xu, M. Chen, and H. Wu, "Three-dimensional memristive Hindmarsh–Rose neuron model with hidden coexisting asymmetric behaviors," *Complexity*, vol. 2018, Feb. 2018, Art. no. 3872573.
- [36] C. Wang and Q. Ding, "A new two-dimensional map with hidden attractors," *Entropy*, vol. 20, no. 5, p. 322, 2018.
- [37] J. P. Singh and B. K. Roy, "Hidden attractors in a new complex generalised lorenz hyperchaotic system, its synchronisation using adaptive contraction theory, circuit validation and application," *Nonlinear Dyn.*, vol. 92, no. 2, pp. 373–394, Apr. 2018.
- [38] J. Munoz-Pacheco, E. Zambrano-Serrano, C. Volos, S. Jafari, J. Kengne, and K. Rajagopal, "A new fractional-order chaotic system with different families of hidden and self-excited attractors," *Entropy*, vol. 20, no. 8, p. 564, 2018.
- [39] T. Kapitaniak, S. Mohammadi, S. Mekhilef, F. Alsaadi, T. Hayat, and V.-T. Pham, "A new chaotic system with stable equilibrium: Entropy analysis, parameter estimation, and circuit design," *Entropy*, vol. 20, no. 9, p. 670, 2018.
- [40] S. T. Kingni, V.-T. Pham, S. Jafari, and P. Wofo, "A chaotic system with an infinite number of equilibrium points located on a line and on a hyperbola and its fractional-order form," *Chaos, Solitons Fractals*, vol. 99, pp. 209–218, Jun. 2017.
- [41] G. Chen, N. V. Kuznetsov, G. A. Leonov, and T. N. Mokaev, "Hidden attractors on one path: Glukhovskiy–dolzhansky, lorenz, and rabynovich systems," *Int. J. Bifurcation Chaos*, vol. 27, no. 8, Jul. 2017, Art. no. 1750115.
- [42] X. Hu, C. Liu, L. Liu, J. Ni, and S. Li, "Multi-scroll hidden attractors in improved sprott a system," *Nonlinear Dyn.*, vol. 86, no. 3, pp. 1725–1734, Nov. 2016.
- [43] D. Dudkowski, S. Jafari, T. Kapitaniak, N. V. Kuznetsov, G. A. Leonov, and A. Prasad, "Hidden attractors in dynamical systems," *Phys. Rep.*, vol. 637, pp. 1–50, Jun. 2016.
- [44] S. Vaidyanathan and C. Volos, "Analysis and adaptive control of a novel 3-D conservative no-equilibrium chaotic system," *Arch. Control Sci.*, vol. 25, no. 3, pp. 333–353, Sep. 2015.
- [45] G. A. Leonov, N. V. Kuznetsov, and T. N. Mokaev, "Hidden attractor and homoclinic orbit in lorenz-like system describing convective fluid motion in rotating cavity," *Commun. Nonlinear Sci. Numer. Simul.*, vol. 28, nos. 1–3, pp. 166–174, Nov. 2015.
- [46] A. P. Kuznetsov, S. P. Kuznetsov, E. Mosekilde, and N. V. Stankevich, "Coexisting hidden attractors in a radio-physical oscillator system," *J. Phys. A, Math. Theor.*, vol. 48, no. 12, Mar. 2015, Art. no. 125101.
- [47] Y. Feng and Z. Wei, "Delayed feedback control and bifurcation analysis of the generalized sprott b system with hidden attractors," *Eur. Phys. J. Special Topics*, vol. 224, no. 8, pp. 1619–1636, Jul. 2015.
- [48] G. A. Leonov, N. V. Kuznetsov, M. A. Kiseleva, E. P. Solovyeva, and A. M. Zaretskiy, "Hidden oscillations in mathematical model of drilling system actuated by induction motor with a wound rotor," *Nonlinear Dyn.*, vol. 77, nos. 1–2, pp. 277–288, Jul. 2014.
- [49] G. A. Leonov, N. V. Kuznetsov, and V. I. Vagaitsev, "Localization of hidden Chua's attractors," *Phys. Lett. A*, vol. 375, no. 23, pp. 2230–2233, 2011.
- [50] C. Li, W. Hu, J. C. Sprott, and X. Wang, "Multistability in symmetric chaotic systems," *Eur. Phys. J. Special Topics*, vol. 224, no. 8, pp. 1493–1506, Jul. 2015.
- [51] M. Borah, "On coexistence of fractional-order hidden attractors," *J. Comput. Nonlinear Dyn.*, vol. 13, no. 9, Sep. 2018, Art. no. 090906.
- [52] L. Liu, C. Du, X. Zhang, J. Li, and S. Shi, "Dynamics and entropy analysis for a new 4-D hyperchaotic system with coexisting hidden attractors," *Entropy*, vol. 21, no. 3, p. 287, 2019.
- [53] V. Varshney, S. Sabarathinam, A. Prasad, and K. Thamilmaran, "Infinite number of hidden attractors in memristor-based autonomous duffing oscillator," *Int. J. Bifurcation Chaos*, vol. 28, no. 01, Jan. 2018, Art. no. 1850013.

- [54] H. Bao, W. Liu, and M. Chen, "Hidden extreme multistability and dimensionality reduction analysis for an improved non-autonomous memristive FitzHugh–Nagumo circuit," *Nonlinear Dyn.*, vol. 96, no. 3, pp. 1879–1894, May 2019.
- [55] L. Liu, C. Du, L. Liang, and X. Zhang, "A high spectral entropy (SE) memristive hidden chaotic system with multi-type quasi-periodic and its circuit," *Entropy*, vol. 21, no. 10, p. 1026, 2019.
- [56] G. L. Wang, Y. C. Lai, and C. Grebogi, "Transient chaos—a resolution of breakdown of quantum-classical correspondence in optomechanics," *Sci. Rep.*, vol. 6, Oct. 2016, Art. no. 35381.
- [57] X.-S. Yang and Q. Yuan, "Chaos and transient chaos in simple hopfield neural networks," *Neurocomputing*, vol. 69, nos. 1–3, pp. 232–241, Dec. 2005.
- [58] R. S. T. Lee, "A transient-chaotic autoassociative network (TCAN) based on lee oscillators," *IEEE Trans. Neural Netw.*, vol. 15, no. 5, pp. 1228–1243, Sep. 2004.
- [59] A. Hoff, D. T. da Silva, C. Manchein, and H. A. Albuquerque, "Bifurcation structures and transient chaos in a four-dimensional chua model," *Phys. Lett. A*, vol. 378, no. 3, pp. 171–177, Jan. 2014.
- [60] S. Sabarathinam and K. Thamilmaran, "Transient chaos in a globally coupled system of nearly conservative Hamiltonian duffing oscillators," *Chaos, Solitons Fractals*, vol. 73, pp. 129–140, Apr. 2015.
- [61] S. Bhalekar, V. Daftardar-Gejji, D. Baleanu, and R. Magin, "Transient chaos in fractional bloch equations," *Comput. Math. Appl.*, vol. 64, no. 10, pp. 3367–3376, Nov. 2012.
- [62] J. Duarte, C. Januário, N. Martins, and J. Sardanyés, "On chaos, transient chaos and ghosts in single population models with allee effects," *Nonlinear Anal., Real World Appl.*, vol. 13, no. 4, pp. 1647–1661, Aug. 2012.
- [63] P. Naseradinmousavi and C. Nataraj, "Transient chaos and crisis phenomena in butterfly valves driven by solenoid actuators," *Commun. Nonlinear Sci. Numer. Simul.*, vol. 17, no. 11, pp. 4336–4345, Nov. 2012.
- [64] A. S. de Paula, M. A. Savi, and F. H. I. Pereira-Pinto, "Chaos and transient chaos in an experimental nonlinear pendulum," *J. Sound Vibrat.*, vol. 294, no. 3, pp. 585–595, Jun. 2006.
- [65] O. Z. Didenko and P. E. Strizhak, "Effect of temperature and small amounts of metal ions on transient chaos in the batch Belousov–Zhabotinsky system," *Chem. Phys. Lett.*, vol. 340, nos. 1–2, pp. 55–61, May 2001.
- [66] H. Dai, X. Yue, J. Yuan, D. Xie, and S. Atluri, "A comparison of classical Runge-Kutta and Henon's methods for capturing chaos and chaotic transients in an aeroelastic system with freeplay nonlinearity," *Nonlinear Dyn.*, vol. 81, nos. 1–2, pp. 169–188, Jul. 2015.
- [67] H. Dai, X. Yue, D. Xie, and S. N. Atluri, "Chaos and chaotic transients in an aeroelastic system," *J. Sound Vibrat.*, vol. 333, no. 26, pp. 7267–7285, Dec. 2014.
- [68] B. C. Bao, P. Jiang, H. G. Wu, and F. W. Hu, "Complex transient dynamics in periodically forced memristive Chua's circuit," *Nonlinear Dyn.*, vol. 79, no. 4, pp. 2333–2343, Mar. 2015.
- [69] K. Buszko and K. Stefański, "Measuring transient chaos in nonlinear one-and two-dimensional maps," *Chaos, Solitons Fractals*, vol. 27, no. 3, pp. 630–646, Feb. 2006.
- [70] T. Lilienkamp and U. Parlitz, "Terminal transient phase of chaotic transients," *Phys. Rev. Lett.*, vol. 120, no. 9, Feb. 2018, Art. no. 094101.
- [71] T. Tél and Y.-C. Lai, "Chaotic transients in spatially extended systems," *Phys. Rep.*, vol. 460, no. 6, pp. 245–275, May 2008.
- [72] H. Y. Shu, L. Wang, and J. Watmough, "Sustained and transient oscillations and chaos induced by delayed antiviral immune response in an immunosuppressive infection model," *J. Math. Biol.*, vol. 68, nos. 1–2, pp. 477–503, Jan. 2014.
- [73] C. T. Bauch and D. J. D. Earn, "Transients and attractors in epidemics," *Proc. Roy. Soc. London. B, Biol. Sci.*, vol. 270, no. 1524, pp. 1573–1578, Aug. 2003.
- [74] Z. Chen and F. Chen, "Complex aperiodic mixed mode oscillations induced by crisis and transient chaos in a nonlinear system with slow parametric excitation," *Nonlinear Dyn.*, vol. 100, no. 1, pp. 659–677, Mar. 2020.
- [75] X. Huang, J. Jia, Y. Li, and Z. Wang, "Complex nonlinear dynamics in fractional and integer order memristor-based systems," *Neurocomputing*, vol. 218, pp. 296–306, Dec. 2016.
- [76] A. Wolf, J. B. Swift, H. L. Swinney, and J. A. Vastano, "Determining Lyapunov exponents from a time series," *Phys. D, Nonlinear Phenomena*, vol. 16, no. 3, pp. 285–317, Jul. 1985.
- [77] S. He, K. Sun, and H. Wang, "Complexity analysis and DSP implementation of the fractional-order lorenz hyperchaotic system," *Entropy*, vol. 17, no. 12, pp. 8299–8311, 2015.



CHUANHONG DU received the B.S. degree in measurement and control technology and instrument from the Harbin University of Science and Technology, Harbin, China, in 2005, and the M.S. degree in circuit and system from Harbin Engineering University, Harbin, in 2013. She is currently a Lecturer with the School of Electronic and Information Engineering, Anshun University, Anshun, China. Her research interests include chaotic systems, circuit design and application for chaotic systems, and chaotic synchronization.



LICAI LIU (Member, IEEE) received the B.S. degree in electronic information engineering from Bayi Agricultural University, Daqing, China, in 2008, and the M.S. degree in communication and information system from Harbin Engineering University, Harbin, China, in 2013. He is currently a Lecturer with the School of Electronic and Information Engineering, Anshun University, Anshun, China. His research interests include chaotic systems and circuit design and application for nonlinear chaotic systems.



SHUAISHUAI SHI received the B.S. degree in electronic information engineering from Zaozhuang University, Zaozhuang, China, in 2012, and the M.S. degree in electronic science and technology from Harbin Engineering University, Harbin, China, in 2015. He is currently a Lecturer with the School of Information Engineering, Guizhou University of Engineering Science, Bijie, China. His research interests include chaotic switched systems and chaotic secure communications.



YONG WEI received the B.S. degree in electrical and information engineering from the Jiangnan Petroleum Institute, China, in 2003, and the M.S. degree in signal and information processing and the Ph.D. degree in geodetection and information technology from Yangtze University, Jingzhou, China, in 2006 and 2016, respectively. He was a Lecturer with the Department of Automation, Yangtze University, from September 2006 to August 2016. Since 2016, he has been an Associate Professor with the Department of Measurement and Control Technology and Instrumentation, Yangtze University. From October 2018 to October 2019, he was a Visiting Scholar with the University of Houston, Houston, TX, USA. His main research interests include chaos and new method and instrument for acoustic and electric well logging.

• • •